

Influence of microstructural size on the thermal shock behavior of Al₂O₃-Er₃Al₅O₁₂ directionally solidified eutectics.

Ying Nie^{#,§}, Patricia B. Oliete[#] and Rosa I. Merino^{*,#}

[#]Instituto de Ciencia de Materiales de Aragón, CSIC – Universidad de Zaragoza

Pedro Cerbuna 12, 50009 Zaragoza, Spain

[§]Present Address: Center for Composite Materials, Harbin Institute of Technology, Harbin 150080, China

* corresponding author. E-mail: rmerino@unizar.es

Declarations of interest: none

Keywords: Eutectic Solidification, Ceramic Composites, Fracture, Thermal Shock

Abstract

We analyze the thermal shock resistance of directionally solidified eutectics. When quenching in water, the resistance starts to deteriorate with temperature differences in the range 260 to 300 K, almost independent of the microstructure size (or initial flexural strength). Unlike other strong, dense ceramics, the loss of strength is gradual upon quenching in boiling water. The onset of crack propagation seems to be controlled by the mismatch of the thermal and elastic properties of the component phases, while the length of the propagated cracks is limited by their quantity, which is estimated to scale approximately with the interface density.

doi published manuscript: 10.1016/j.scriptamat.2018.09.036

© 2018 This manuscript version is made available under the CC-BY-NC-ND 4.0

license <http://creativecommons.org/licenses/by-nc-nd/4.0/>

Ying Nie^{#,§}, Patricia B. Oliete[#] and Rosa I. Merino^{*,#}

[#]Instituto de Ciencia de Materiales de Aragón, CSIC – Universidad de Zaragoza

Pedro Cerbuna 12, 50009 Zaragoza, Spain

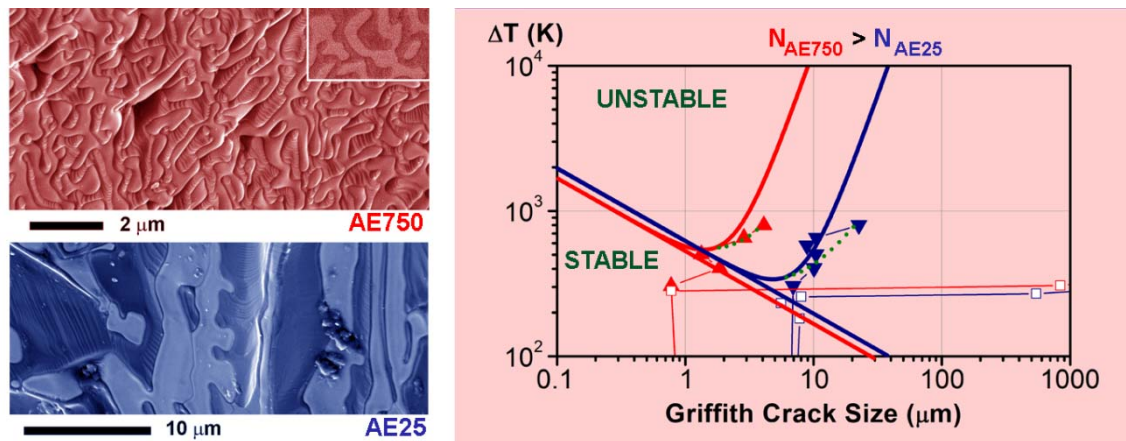
[§]Present Address: Center for Composite Materials, Harbin Institute of Technology, Harbin 150080, China

* corresponding author. E-mail: rmerino@unizar.es

Declarations of interest: none

Keywords: EUTECTIC SOLIDIFICATION, CERAMICS, COMPOSITES, FRACTURE, THERMAL SHOCK

Graphical Abstract



In the recent decades, Al₂O₃-based eutectic ceramics have received much attention as structural materials, particularly because of excellent microstructural and chemical stability, creep resistance and mechanical strengths in high-temperature oxidizing atmosphere [1-8]. Very high values of flexural strength have been observed. Flexural strength increases with decreasing interphase spacing (λ), being proportional to $\lambda^{-1/2}$. The high strength comes about by the homogeneous two-phase microstructure with fine control over the microstructural size that is achieved by directional solidification procedures, together with strongly bonded interphases. Alumina-rare earth garnet eutectics present also selective emissivity and have been proposed and investigated as selective thermal emitters for thermophotovoltaic devices. [9-12] Appropriate thermal stress resistance is required in the aforementioned application, but the detailed study of the thermal shock behavior has not been performed previously.

Experiments to measure thermal emission done by laser heating rods of the material up to 1600 °C, which were followed by fast cooling in ambient air, show that they can support moderate thermal shock conditions without apparent degradation. Al₂O₃-aluminium garnet directionally solidified eutectics have typically a high degree of brittleness (with $K_{IC} \approx 2 \text{ MPam}^{1/2}$), relatively low thermal conductivity, and high Young's modulus, being susceptible to catastrophic failure under severe thermal transients [13]. The purpose of this work is to study, using standard quenching test methods, the thermal shock behavior of directionally solidified Al₂O₃-Er₃Al₅O₁₂ eutectic selective emitters with emphasis on the microstructural size dependence. The outcome will be applicable to similar alumina-garnet eutectics.

Ceramic feed rods with the eutectic composition of 81mol% Al_2O_3 + 19 mol% Er_2O_3 were prepared by mixing, compaction and sintering of the Al_2O_3 (Aldrich 99.99%), Er_2O_3 (Alfa Aesar 99.99%) powders, similarly as elsewhere [7]. Eutectic rods of diameters 1.2 to 1.6 mm were directionally solidified from the melt in nitrogen atmosphere [14] by the laser floating zone method at 25mm/h and 750mm/h processing rates. The solidified samples had an interpenetrated microstructure of Al_2O_3 and $\text{Er}_3\text{Al}_5\text{O}_{12}$ phases. The values of interphase spacing measured by the line interception method are given in table I.

The rods were cut to a length of 45 mm and both cross-sections were carefully polished for thermal shock tests. As the severity of the thermal shock depends on the sample size and the properties of the quenching media and heat transfer coefficient (h), [15-18] here we have always used cylindrical-rod shaped samples with similar sizes (diameters from 1.2 to 1.6 mm) and we have done quenching experiments in both, room temperature (RT) and boiling water. The thermal shock resistance was assessed by measuring the retained flexural strength of the samples after quenching from a given holding temperature into large volume baths of RT water ($T = 18^\circ\text{C}$ to 20°C) or boiling ($T = 95^\circ\text{C}$) water. The test specimen temperature was maintained at least 15 min before quenching and then transferred to the quenching bath within 3s.[19] Three-point flexural tests were carried on Electronic Universal Testing Machine (Instron 5565, UK), with a span of 16 mm and 30 $\mu\text{m}/\text{min}$ strain rate. A minimum number of three valid data were measured to calculate the average flexural strength. [5] Microstructure and fracture surfaces were observed by Scanning Electron Microscopy (MERLIN Field Emission Scanning Electron Microscope (FE-SEM) from Carl Zeiss).

Fig. 1 shows the retained flexural strengths together with the corresponding standard errors of Al₂O₃/EAG eutectics solidified at 25 mm/h (denoted AE25 from now on) and 750 mm/h (AE750) as a function of thermal shock total temperature difference ($\Delta T = T_{\text{hold}} - T_{\text{bath}}$). The samples quenched in RT water show a sharp, catastrophic degradation of strength at $\Delta T = \Delta T_c = 260$ K (AE25) and $\Delta T_c = 290$ K (AE750). According to the unified theory presented by Hasselman [13, 20], this is the expected behavior of strong ceramics, with very small initial cracks (flaws). Once a short crack starts to propagate at a critical temperature difference, it continues propagating kinetically. Crack propagation continues longer for smaller initial flaws, and causes a sharp drop of strength. The original strength of AE750 was 2.2 to 2.6 times higher than that of AE25, as usual for this material [5] but the ΔT_c of AE750 was only 1.1 times the one of AE25.

Figure 1 shows also the retained flexural strength of the samples upon quenching in boiling water versus temperature difference. The degradation of flexural strength is more gradual. The 3-point flexure load-displacement curves registered to measure the retained strength had the same slope as before the quenching, compatible with Young's modulus values equal to the one of the as-grown samples [5]. Therefore, there is no extensive cracking of the samples even if their retained strength has clearly diminished. Fracture surfaces of quenched specimens, showing brittle fracture, are given in figure 2, a and b for AE25, c and d for AE750. All the observed surfaces are similar: the fracture initiates at the surface, without evidence of changes in the way the cracks propagate between quenched and unquenched samples. The absence of catastrophic failure in the specimens quenched into boiling water is to be associated to the different ways of heat transfer in both procedures.[17] Upon quenching in RT water, the heat flux is far larger

and less homogeneous, favoured by a transient regime with vigorous boiling and solid-liquid bubble contacts.

From the values of the retained flexural strength, we have estimated the radius of the critical flaw size after thermal shock (figure 3) using expression 1[3]

$$a = \frac{1}{\pi} \left[\frac{K_{IC}}{0.65\sigma} \right]^2 \quad (1)$$

K_{IC} is the fracture toughness. Clearly, when the critical flaw size is of the order of 1 mm, the samples have lost all their strength ($\Delta T > \Delta T_C$ in RT water). Upon quenching in boiling water, as ΔT increases we observe a gradual increase in the size of the critical flaw, starting from values of the order of the phase size of the eutectic composite. Moreover, the cracks start to propagate at about the same ΔT in both composites, irrespective of which was the size of this initial flaw.

A so similar value for ΔT_C (quenching in RT water) or ΔT to start to propagate cracks (boiling water), for both samples might seem surprising for composites with so different flexural strength. The critical temperature to initiate fracture in a rod of material subjected to severe thermal quenching is determined by the thermal shock resistance parameter R , equation (2), which for rod shaped samples is given by the temperature decrease causing a thermal tensile stress equal to the sample strength (σ_f) [13, 15, 21-23],

$$R = \frac{\sigma_f(1-\nu)}{\alpha E} \quad (2)$$

where σ_f is the fracture resistance, ν the Poisson's ratio, α the thermal expansion coefficient and E the Young's modulus. Calculated R values for AE25 and AE750 are

240 K and 530 K (see table I). While the R value for AE25 is near to the corresponding ΔT_C (quenching in RT water) or ΔT to start to propagate cracks (boiling water) found experimentally, ΔT_C for AE750 is much smaller than its R value. It is well known that strong and fragile ceramics tend to show catastrophic rupture under severe thermal quenching, very frequently with temperature quenching differences smaller than the calculated R parameter. Therefore, instead of increasing strength, the strategy to increase the thermal shock resistance to damage of strong ceramics is to minimize the extent of crack propagation.[13, 20, 24-27] Often this is done by introducing second phase particles (or microstructural inhomogeneities) into the matrix that increase the toughness and/or decrease the Young's modulus of the material [13, 22] and slow crack propagation. These inhomogeneities also concentrate thermal stress at the second phase leading to microcracking and avoiding catastrophic failure.[28-31]

The present directionally solidified eutectic is already a two-phase material, whose microstructural distribution and size do not affect to its fracture toughness or Young's modulus, but can contribute to its thermal shock behavior through the inhomogeneity of the thermomechanical properties associated to the two-phase material. Upon quenching, each phase will experience a different time-dependent thermal contraction, according to their different thermal expansion, thermal conductivity, and elastic constants. Stresses larger than the ones corresponding to the homogenized body and large enough to initiate fracture could develop at the interfaces during the transients due to mismatch in thermal properties of the adjacent phases, as suggested by Zimmerman [32] in SiC-ZrB₂ composites.

In the tests performed, the volume of sample subjected to the fastest temperature variation is the one adjacent to the outer surface, therefore we need to pay attention to its microstructure. It is given in figure 2, third row (e, f). It can be seen that the feature sizes are equal on the surface and inside the material. One can also see that the as-grown sample surfaces are slightly grooved at the interfaces between Al_2O_3 and $\text{Er}_3\text{Al}_5\text{O}_{12}$. We propose that microcracks will start to grow at these interfaces, in the volume of material subjected to fast thermal transients, until they reach a size comparable to the microstructural size. With this model, the ΔT at which the cracks start to grow (or equivalently the material strength start to deteriorate) would not be determined by the properties of the homogenized material (composite), but should be highly influenced by the mismatch in the elastic and thermoelastic properties of the components (Al_2O_3 and EAG). Therefore, it is expected that the temperature at which cracks start to propagate is similar in both composites, as observed experimentally. Once the cracks start to grow, they continue across both phases (fracture is mainly transgranular [5]) in the thermal stress field towards the interior of the material, according to the homogenized averaged thermomechanical properties of the brittle composite and the severity of the thermal shock.

The cracks stop, under the energy approximation [20], when the accumulated elastic energy has been dissipated by the formation of new crack surfaces. A large number of cracks help to dissipate accumulated elastic energy with shorter propagated cracks.

Hasselman gave expressions for the size of a propagated crack (l_f) considering a brittle material composed of N Griffith microcracks per unit volume of initial crack length l_0 . Once the cracks start to propagate (at a ΔT large enough to enter the instability region),

they will grow until the potential energy released equals the total surface fracture energy. This is expressed in Eq. 3 [20].

$$\frac{3(\alpha\Delta T)^2 E_0}{2(1-2\nu)} \left\{ \left[1 + \frac{16(1-\nu^2)Nl_0^3}{9(1-2\nu)} \right]^{-1} - \left[1 + \frac{16(1-\nu^2)Nl_f^3}{9(1-2\nu)} \right]^{-1} \right\} = 2\pi NG(l_f^2 - l_0^2) \quad (3)$$

We have used this equation to fit the critical flaw size (or final crack length after thermal shock, l_f) vs ΔT in Figure 3 (data from quenching in boiling water), and using the values given in Table I for the homogenized composite (α , ν and $E_0=E$ and approximating the surface fracture energy, G , by K_{IC}^2/E). The fitted N values are: for AE750, with $l_0 = 0.95 \mu\text{m}$, $N \approx 2.3 \times 10^{16} \text{ m}^{-3}$; and for AE25, with $l_0 = 6.12 \mu\text{m}$, $N \approx 5.5 \times 10^{14} \text{ m}^{-3}$. The short-dash lines in Figure 3 show the fit. Note that the density of propagating cracks is larger in AE750 than in AE25. The distance between adjacent propagating cracks can be estimated by $N^{-1/3}$, which amounts to $3.5 \mu\text{m}$ for AE750 and $12.2 \mu\text{m}$ for AE25. This is of the order of the microstructure size and indicates that it is a reasonable assumption to consider that cracks do propagate from interphase junctions where maximum transient thermal stresses develop.

Further, this picture is consistent with the Hasselman unified theory if one attends to the area of crack instability that can also be calculated for the homogenized body with the same set of parameters and equation 4 from reference 20 (see inset in figure 3). The crack instability region is bound by a concave curve in a ΔT versus crack length plot, with minima at points ($l = 1.4 \mu\text{m}$, $\Delta T = 540 \text{ K}$) for AE750 and ($l = 4.9 \mu\text{m}$, $\Delta T = 340 \text{ K}$) for AE25. Upon a temperature difference of $\Delta T = 300 \text{ K}$, both AE25 and AE750 materials stay in the stable region, with Griffith crack size near to or even to the right of the minimum of the stability curves. Upon $\Delta T \approx 400 \text{ K}$ in boiling water, cracks propagating from interphase regions grow up to approximately twice its initial size.

These larger cracks bring the ΔT vs crack size points further to the right of the minimum of the instability curve, still inside the stable region. With even larger ΔT (clearly the points above 650 K for AE750 or at 800 K for AE25), the homogenized body unstable crack region is entered and the cracks grow further (points lying onto the dashed line, l_f).

Upon quenching in RT water, the number of propagating cracks is smaller, as suggested by its larger final size. If one relies on the l_f values given in Figure 3 and using equation 3, the density of propagating cracks is of the order of 10^{11} m^{-3} for both materials.

Therefore, immediately after the cracks start to propagate from interphase boundaries, or at $\Delta T \approx R$ in AE25, they enter the unstable region and propagate catastrophically up to sizes larger than the sample transverse size. AE25 enters the unstable region at a ΔT given by R , which is a bit smaller than the ΔT that would trigger crack growth due to the mismatch of thermal parameters between components of the composite AE750. The unstable-stable boundary is indicated by small dotted lines in the inset of figure 3. The smaller density of propagating cracks upon quenching in RT water is in accord with bubble formation and burst of boiling that increase h very severely at discrete points onto the samples surfaces.

To conclude, it is worth to remark that the results and analyses presented here show that $\text{Al}_2\text{O}_3\text{-Er}_3\text{Al}_5\text{O}_{12}$ eutectics with finer microstructure are better, not only when high flexural strength is required, but under circumstances where relatively mild thermal shock conditions are to be found. These mild conditions are represented in the manuscript by quenching in boiling water, but will include also free cooling in air of selective emitters. The reason for the better response of fine micro-structured, strong

eutectics over coarser ones resides on the first having a larger amount of propagating thermal cracks from Al_2O_3 - $\text{Er}_3\text{Al}_5\text{O}_{12}$ interface boundaries. It is important to emphasize also that to rank eutectics of this kind for thermal shock resistance, which possess large flexural strength, one should prioritize minimum mismatch of the thermal conductivity and thermal expansion values among the component phases, together with large thermal stress stability parameter ($R_{\text{st}} = K_{\text{IC}}/\alpha E$). This would increase the temperature difference at which the cracks start to grow and diminish the final size of the propagated cracks, respectively.

Acknowledgements

This work has been supported by the Spanish Ministerio de Economía, Industria y Competitividad (MINECO) and the CE (FEDER Funds) [grants number MAT2013-41045-R-EMITEME and MAT-2016-77769R-FLASCERAMAT]. Authors would like to acknowledge the Servicio General de Apoyo a la Investigación-SAI, Universidad de Zaragoza. Y. Nie would like to acknowledge the China Scholarship Council for a funding of Doctoral Joint-Training Program. We also thank Prof. V.M. Orera for critical reading of the manuscript.

Table I. Values of thermomechanical parameters for AE25, AE750. R has been calculated using equation 2, the flexural strength data given in the table (first column) and the following values for $E = 311 \text{ GPa}$ [5], coefficient of thermal expansion $\alpha = 7.3 \times 10^{-6} \text{ K}^{-1}$ [33-35], and $\nu = 0.24$ [34, 36, 37].

Material	Flexural Strength (MPa)	Fracture Toughness (MPam ^{1/2}) [5]	Interphase spacing (μm)	R (K)	Measured ΔT_c (K)
AE750	1580 ± 280	1.8 ± 0.2	0.71 ± 0.1	530	290
AE25	710 ± 60	2.1 ± 0.3	5.1 ± 1.2	240	260

References

- [1] Y. Waku, N. Nakagawa, T. Wakamoto, H. Ohtsubo, K. Shimizu and Y. Kohtoku, J. Mater. Sci. 33 (1998) 1217-1225.
- [2] J. Martínez Fernández, A. Sayir and S.C. Farmer, Acta Materialia 51 (2003) 1705-1720.
- [3] J. Y. Pastor, J. LLorca, A. Salazar, P.B. Oliete, I. de Francisco and J.I. Peña, J. Am. Ceram. Soc. 88 (2005) 1488–1495.
- [4] J. LLorca and V. M. Orera, Prog. Mater. Sci. 51 (2006) 711–822.
- [5] M. C. Mesa, P. B. Oliete, V. M. Orera, J.Y. Pastor, A. Martín and J. LLorca, J. Eur. Ceram. Soc. 31 (2011) 1241–1250.
- [6] L. Perrière, R. Valle, N. Carrère, G. Gouadec, Ph. Colomban, S. Lartigue-Korinek, L. Mazerolles and M. Parlier. J. Europ. Ceram. Soc. 31 (2011) 1199-1210.
- [7] M.C. Mesa, P.B. Oliete and A. Larrea, J. Crystal Growth 360 (2012) 119-121.
- [8] Q. Ren, H. Su, J. Zhang, W. Ma, B Yao, L. Liu and H. Fu. Scripta Materialia 125 (2016) 39-43.
- [9] N. Nakagawa, H. Ohtsubo, Y. Waku and H. Yugami, J. Eur. Ceram. Soc. 25 (2005) 1285–1291.
- [10] M.C. Mesa, P.B. Oliete, R.I. Merino and V.M. Orera, J. Eur. Ceram. 33 (2013) 2587–2596.
- [11] P.B. Oliete, M.C. Mesa, R.I. Merino and V.M. Orera, Sol. Energy Mater. Sol. Cells 144 (2016) 405–410.
- [12] P.B. Oliete, A. Orera, M.L. Sanjuán and R.I. Merino, Sol. Energy Mater. Sol. Cells 174 (2018) 460-468.
- [13] H. Wang and R. N. Singh, Int. Mater. Rev. 39 (1994) 228–244.

- [14] P. B. Oliete and J. I. Pena, J. Cryst. Growth, 304(2007) 514–519.
- [15] M. Ishitsuka, T. Sato, T. Endo and M. Shimada, J. Mater. Sci. 24(1989) 4057–4061.
- [16] L. M. Chen, F. Zhu, Z. J. Zhang, P. Hu, A.Z. Wang, Y.H. Ling, W. Liang, X.B. Suo and X.H. Zhang, Journal of Alloys and Compounds 724 (2017) 234–239.
- [17] Y. Lee, T. J. McKrell and M. S. Kazimi, J. Nucl. Mater. 467 (2015) 172–180.
- [18] P. F. Becher, J. Am. Ceram. Soc. 1-1 (1981) C17–C18.
- [19] Standard Test Method for Determination of Thermal Shock Resistance for Advanced Ceramics by Water Quenching, ASTM C1525–04.
- [20] D.P. H. Hasselman, J. Am. Ceram Soc. 52 (1969) 600-604.
- [21] W.D. Kingery, J. Am. Ceram. Soc. 38 (1955) 3-15.
- [22] C. Aksel and P. D. Warren, J. Eur. Ceram. Soc. 23 (2003) 301–308.
- [23] H. Hencke, J.R. Thomas Jr and D.P.H. Hasselman. J. Am. Ceram. Soc. 67 (1984) 393-398.
- [24] D.P. H. Hasselman, J. Am. Ceram Soc. 53 (1970) 490-495.
- [25] D.P. H. Hasselman, Ceram. Int. 4 (1978) 147-150.
- [26] G.A. Schneider, Ceram. Int. 17 (1991) 325-333.
- [27] Z.H. Zhang, Z. Wang, P. Hu, W.B. Han and C.Q. Hong, Scripta Materialia 61 (2009) 809-812.
- [28] D.P.H. Hasselman, J. Am. Ceram. Soc. 52 (1969) 288-289.
- [29] D.P. H. Hasselman, P.F. Becher and K.S. Mazdiasni, Z. Werkstofftech 11 (1980) 82-92.
- [30] J.W. Zimmermann, G.E. Hilmas and W.G. Fahrenholtz, J. Am. Ceram. Soc. 92 (2009) 161-166.
- [31] R. Uribe and C. Baudín, J. Am. Ceram. Soc. 86 (2003) 846-850.

- [32] J.W. Zimmermann, G.E. Hilmas and W.G. Farenholtz, Mat. Chem. Phys. 112 (2008) 140-145.
- [33] Calculated as a weighted average of the thermal expansion from RT to 300 °C (573K) of Al₂O₃ and Er₃Al₅O₁₂.
- [34] R.G. Munro, J. Am. Ceram. Soc. 80 (1997) 1919-1928.
- [35] K.L. Ovanesyan, A.G. Petrosyan, G. O. Shirinyan and A.A. Avetisyan, Inorg. Mater 17 (1981) 308-315.
- [36] Weighted average of RT values of Poisson's ratio of Al₂O₃ and YAG (assumed isotropic).
- [37] P.R. Stoddart, P.E. Ngoepe, P.M. Mjwara, J.D. Comins and G.A. Saunders, J. Appl. Phys. 73 (1993) 7298-7301.

Figure 1. Retained strength of AE25 (open symbols) and AE750 (closed symbols) as a function of total temperature difference (ΔT), after quenching in water baths at RT (squares) or boiling (circles). When error bars are given, the value corresponds to averages of at least 3 valid measurements of 3-point flexural strength.

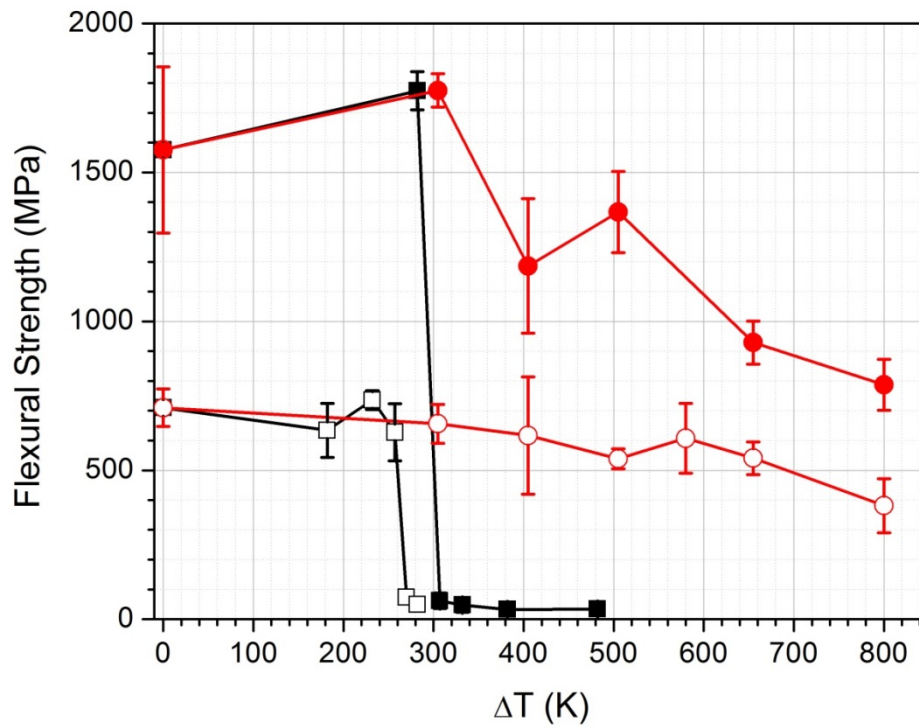


Figure 2. SEM micrographs of fracture surfaces and outer surfaces of samples AE25 and AE750 as grown or after quenched in boiling water. Fracture surfaces of AE25 quenched with $\Delta T = 580$ K (a and b), and AE750 quenched with $\Delta T = 655$ K (c and d). Micrographs e and f are SEM images of the outer surface of AE25 after quenching with $\Delta T = 305$ K (e) and AE750 as grown (f). The dark phase is Al_2O_3 , the bright one is $\text{Er}_3\text{Al}_5\text{O}_{12}$ (see compositional contrast image overlapped and matched in the inset of figure (f)). In (f) and (e) the surface of Al_2O_3 shows steps.

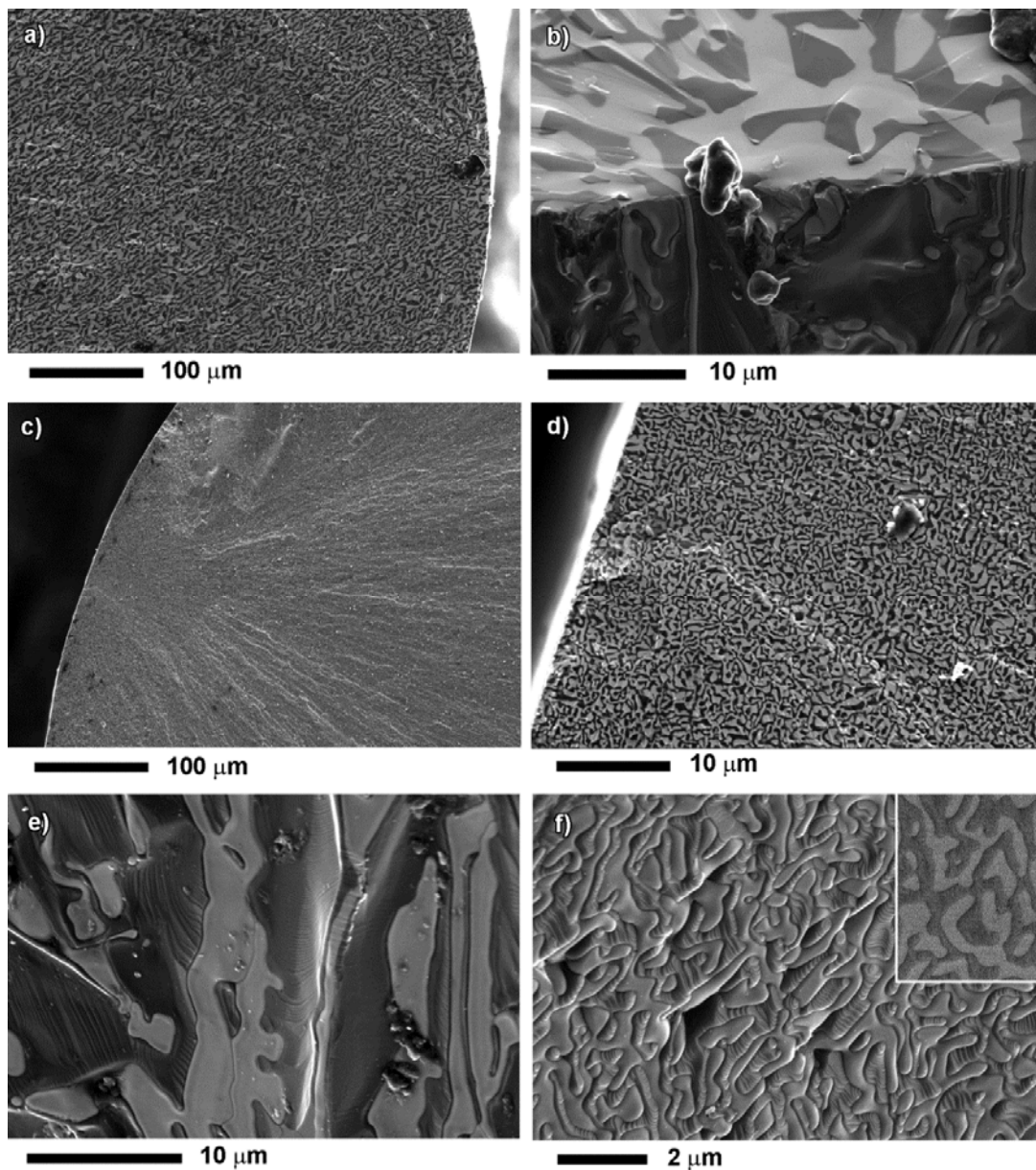


Figure 3. MAIN PLOT: Critical defect size calculated with equation 1, using as K_{IC} the values given in table I for each composite, and as σ_f the measured retained strength. AE25 (open symbols) and AE750 (closed symbols); after quenching in water baths at RT (squares) or boiling (circles). The dashed lines are fitted curves to the final crack length as explained in the text. INSET: The curves in the inset show the critical temperature difference for the initiation of crack propagation according to Hasselman Unified Theory and the parameter values indicated in the text. Concave continuous lines apply for quenching in boiling water; small dotted straight lines apply for quenching in RT water. Symbols and dash-lines as in the main plot.

